

# Comparison of Hadronic Interaction Models at Auger Energies

D. Heck<sup>a\*</sup>, M. Risse<sup>a</sup>, and J. Knapp<sup>b</sup>

<sup>a</sup>Institut für Kernphysik, Forschungszentrum Karlsruhe, P.O. Box 3640, D-76021 Karlsruhe, Germany

<sup>b</sup>Dept. of Physics and Astronomy, University of Leeds, Leeds LS2 9JT, United Kingdom

The three hadronic interaction models DPMJET 2.55, QGSJET 01, and SIBYLL 2.1, implemented in the air shower simulation program CORSIKA, are compared in the energy range of interest for the Pierre Auger experiment. The model dependence of relevant quantities in individual hadronic interactions and air showers is investigated.

## 1. INTRODUCTION

The engineering array of the southern Pierre Auger Observatory (PAO) [3] in Argentina has recently started to take data. The interpretation of the measurements requires reliable numerical simulations of extensive air showers (EAS) in the extremely-high energy (EHE) range  $> 10^{19}$  eV. A large uncertainty in such simulations arises from the models which describe the hadronic interactions. As one has to extrapolate in energy from accelerators by several orders of magnitude and into the forward kinematical range which is unobserved by collider experiments, the models have to rely on theoretical guidelines to describe the EHE collisions. In this contribution model predictions for single interactions of  $p\text{-}\bar{p}$ ,  $p\text{-}^{14}\text{N}$ , and  $\pi\text{-}^{14}\text{N}$  collisions are compared, and we examine how their features influence measurable EAS quantities such as the longitudinal development with the shower maximum  $X_{\text{max}}$  and the lateral distributions of particle densities at ground.

## 2. MODELS

Presently three hadronic interaction codes coupled with the EAS simulation program CORSIKA [8] are able to treat hadronic collisions at energies  $> 10^{19}$  eV: DPMJET 2.55 [12], QGSJET 01 [10,9], and SIBYLL 2.1 [6,5]. In this study NEXUS 2 [4] is partly included despite of its upper limit of  $< 2 \times 10^{17}$  eV recommended

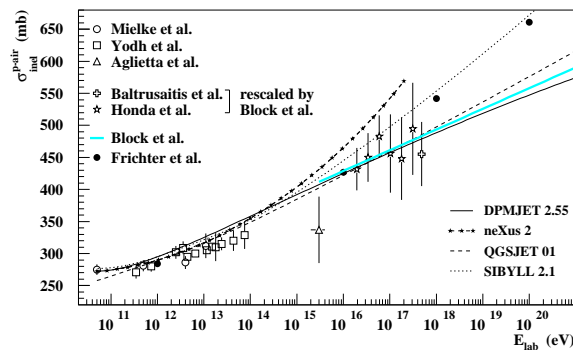


Figure 1. Inelastic proton-air cross-sections of the considered models. Included are experimental data of air shower measurements. Further details see ref. [11].

by its authors. But already at this energy some interesting trends of this model show up. Fig. 1 shows the proton-air cross-sections for production of secondary particles as function of energy.

## 3. SINGLE INTERACTIONS

All models are tuned to reproduce the available collider data. They agree fairly well in the pseudo-rapidity, multiplicity, and transverse momentum distributions obtained by the UA5 [2], CDF [1], and P238 [7] experiments. But when extrapolating to higher energies, already at  $E_{\text{lab}} = 10^{17}$  eV (corresponding to  $\sqrt{s} \approx 14$  TeV, which will be reached by the future LHC-collider), the mid-rapidity density at  $|\eta| < 4$  of QGSJET ex-

\*corresponding author, e-mail: dieter.heck@ik.fzk.de

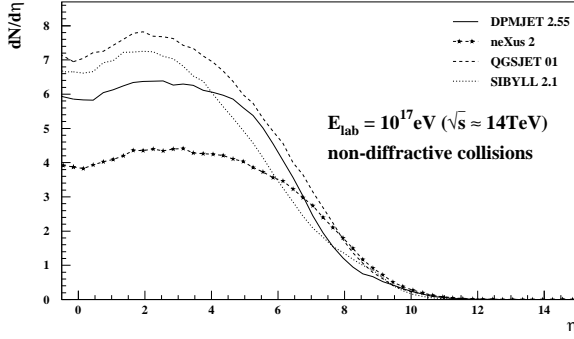


Figure 2. Pseudorapidity distribution of charged particles in  $p\text{-}\bar{p}$  collisions at  $E_{\text{lab}} = 10^{17}$  eV.

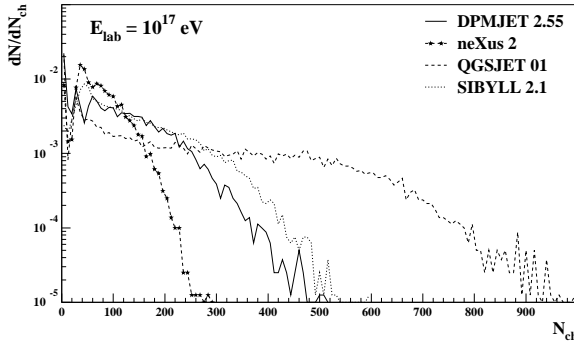


Figure 3. Distribution of charged particle multiplicity in  $\pi\text{-}^{14}\text{N}$  collisions at  $E_{\text{lab}} = 10^{17}$  eV.

ceeds that of NEXUS by up to a factor of  $\approx 2$  as shown in Fig. 2. In Fig. 3 the charged particle multiplicity distribution of  $\pi\text{-}^{14}\text{N}$  collisions shows a similar behaviour. Again QGSJET predictions are higher than those of all other models, while the NEXUS distribution repeats the low multiplicity already shown in the  $p\text{-}\bar{p}$  collisions of Fig. 2. This behaviour reflects the different treatment of the Pomeron exchange by the various models. In QGSJET a hard Pomeron is always coupled to the partons of projectile and target via soft Pomerons, which finally produce the large number of secondary particles. Secondaries produced by cutting soft Pomerons appear in the mid-rapidity range and take away only a minute energy fraction. Therefore they influence the development of charged particle numbers in EAS

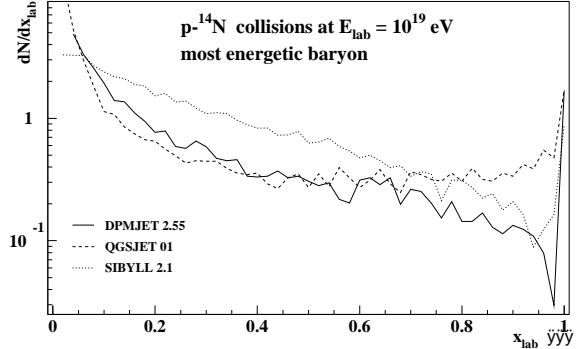


Figure 4. Distribution of longitudinal momentum fraction carried away by the most energetic baryon emerging from  $\pi\text{-}^{14}\text{N}$  collisions at  $E_{\text{lab}} = 10^{19}$  eV.

rather insignificantly.

Already in the calculation of the Pomeron exchange probabilities NEXUS applies strict energy conservation, which reduces the number of cut hard and soft Pomerons, thus reducing the overall multiplicity. This decreases the number of particles emitted in the pseudo-rapidity range below  $|\eta| < 6$  while the fraction of secondaries produced in the very forward direction  $|\eta| > 8$  resembles that of the other considered models.

The distribution of the longitudinal momentum fraction taken away by the leading particle is displayed in Fig. 4. Large differences up to a factor of 10 show up in the diffractive region  $x_{\text{lab}} > 0.8$ , but also around  $x_{\text{lab}} \approx 0.4$  significant deviations are visible. The extremely low probability of DPMJET to produce baryons at  $x_{\text{lab}} \approx 0.97$  in  $\pi\text{-}^{14}\text{N}$  collisions is remarkable. It reflects the insufficient knowledge on high- and low-mass diffraction: Any detailed treatment within the interaction codes is strongly model dependent.

#### 4. INFLUENCE ON EAS FEATURES

In hadronic EAS the  $\pi^\pm$ -mesons are the most frequent secondary hadronic particles and nitrogen is the most abundant component of air. Therefore the character of an EAS is essentially influenced by the features of  $\pi\text{-}^{14}\text{N}$  collisions. In such interactions QGSJET exhibits a lower average elas-

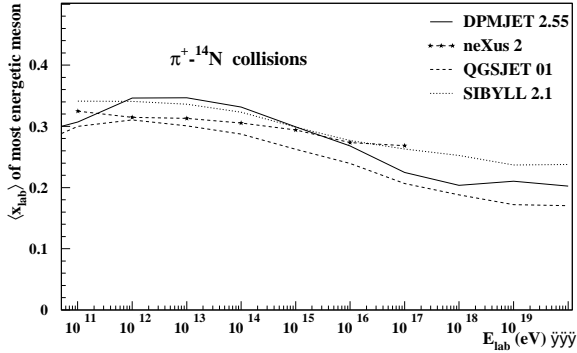


Figure 5. Average of longitudinal momentum fraction carried away by the most energetic meson emerging from  $\pi$ - $^{14}\text{N}$  collisions as function of energy.

ticity than DPMJET and SIBYLL, see Fig. 5. Therefore EAS simulated with QGSJET develop faster than those produced with the other models. The second important influence on the development process arises from the cross-sections. The  $\pi$ -air production cross-sections behave similar to those shown in Fig. 1, but with DPMJET staying well below QGSJET above  $10^{15}$  eV. Therefore EAS simulated with the DPMJET model are expected to develop late, while SIBYLL showers will fall somewhere in between QGSJET and DPM-

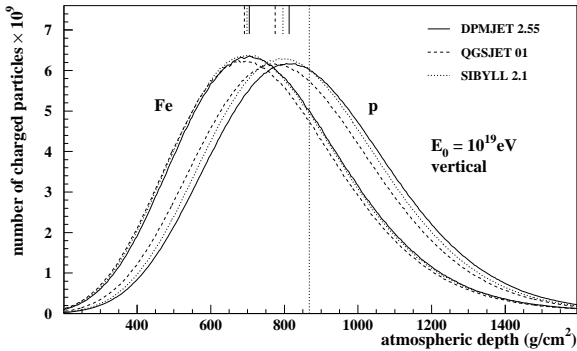


Figure 6. Longitudinal development of charged particle number. Vertical incidence,  $E_0=10^{19}$  eV,  $E_e > 0.1$  MeV. The vertical dotted line indicates the vertical depth of the PAO in Argentina [3].

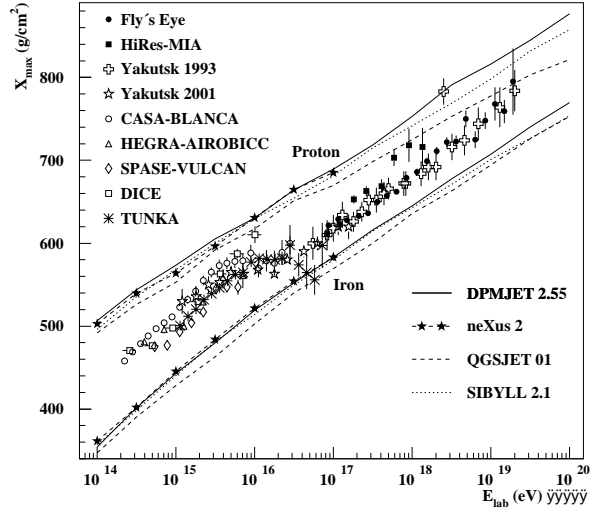


Figure 7. Depth  $X_{max}$  of shower maximum as function of primary energy. Vertical incidence,  $E_0=10^{19}$  eV,  $E_e > 0.1$  MeV. References to experiments (fluorescence = full symbols, Cherenkov techniques = open symbols) are given in [11].

JET. This is demonstrated in Fig. 6 for proton and Iron induced showers of  $10^{19}$  eV. At the upper margin of Fig. 6 the positions of the maxima are indicated. They nearly coincide for Iron induced showers, but for proton induced EAS the difference between QGSJET and DPMJET amounts to  $\approx 40$   $\text{g/cm}^2$ .

The depth of shower maximum  $X_{max}$  as function of primary energy is plotted in Fig. 7. While for Iron induced showers even at highest energies the  $X_{max}$  values coincide within  $< 20$   $\text{g/cm}^2$ , with a tendency of DPMJET to predict deeper penetration, the lines of proton induced showers show a clear divergence with increasing energy reaching 55  $\text{g/cm}^2$  at  $10^{20}$  eV. Especially the QGSJET distribution flattens with increasing energy. Starting at  $10^{15}$  eV with 65  $\text{g/cm}^2$  per energy decade the slope reaches 45  $\text{g/cm}^2$  per decade at  $10^{20}$  eV. The flattening has to be attributed to the lowering of the  $\pi$ - $^{14}\text{N}$  elasticity (Fig. 5) together with an increasing  $\pi$ - $^{14}\text{N}$  cross-section of QGSJET which exceeds that of DPMJET by 10% at  $E_{lab} = 10^{17}$  eV. Above  $10^{15}$  eV the  $X_{max}$  slopes of the other models show no significant change for proton induced EAS.

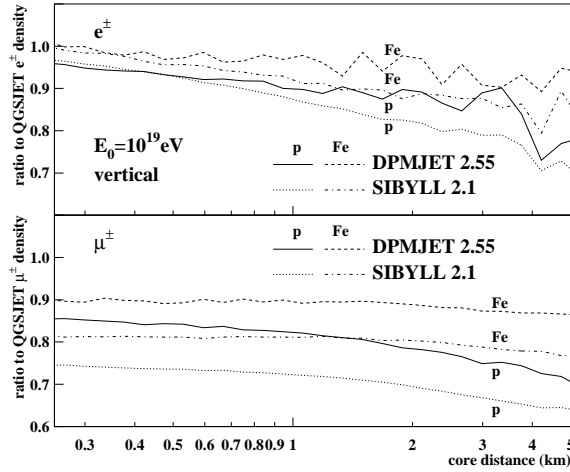


Figure 8. Ratios of lateral particle densities relative to QGSJET. Vertical incidence,  $E_0=10^{19}$  eV,  $\varepsilon_{\text{thin}} = 10^{-6}$  (optimized [13]),  $E_e > 0.25$  MeV,  $E_\mu > 0.1$  GeV.

Because of its early development QGSJET exhibits the flattest lateral distribution for electrons and for muons. This results in the highest particle densities at distances  $> 300$  m not only for proton but also for Iron induced EAS. Therefore we compare in Fig. 8 the lateral distributions of the other models relative to those of QGSJET. With increasing distance from the shower core the densities predicted by the other models are always smaller. The effect is more pronounced for proton induced showers. In general the SIBYLL densities are lowest and the differences are larger for the muon distributions.

## 5. CONCLUSIONS

We emphasize the importance of future collider experiments to measure the very forward range of particle production thus reducing the present uncertainties in EAS simulations caused by the hadronic interaction models. Despite the unknown elemental composition of the primary cosmic radiation at EHE, the PAO should be able to constrain the hadronic interaction models by evaluating hybrid EAS events which combine the longitudinal information measured by fluorescence telescopes and the lateral particle densities reg-

istered by water Cherenkov surface detectors.

## Acknowledgments

Many thanks go to the authors of the hadronic interaction models for their advice in linking their codes with CORSIKA. We thank S. Ostapchenko for enlightening discussions and R. Engel for carefully reading the manuscript. The authors acknowledge support for a British-German Academic Research Collaboration from The British Council and the DAAD.

## REFERENCES

1. F. Abe et al. (CDF Collaboration), *Phys. Rev. Lett.* **61** (1988) 1819; *Phys. Rev.* **D41** (1990) 2330
2. G.J. Alner et al. (UA5 Collaboration), *Phys. Rep.* **154** (1987) 247
3. P. Auger Collaboration, *Pierre Auger Design Report*, Fermilab (1997), <http://www.auger.org/admin/DesignReport/index.html>
4. H.J. Drescher et al., *Phys. Rep.* **350** (2001) 93; *Phys. Rev. Lett.* **86** (2001) 3506
5. R. Engel et al., *Proc. 26<sup>th</sup> Int. Cosmic Ray Conf.*, Salt Lake City (USA) **1** (1999) 415
6. R.S. Fletcher et al., *Phys. Rev.* **D50** (1994) 5710; J. Engel et al., *Phys. Rev.* **D46** (1992) 5013
7. R. Harr et al., *Phys. Lett.* **B401** (1997) 176
8. D. Heck et al., **FZKA 6019**, Forschungszentrum Karlsruhe (1998); see <http://www-ik.fzk.de/~heck/corsika/>
9. D. Heck et al., *Proc. 27<sup>th</sup> Int. Cosmic Ray Conf.*, Hamburg (Germany) **1** (2001) 233
10. N.N. Kalmykov et al., *Nucl. Phys. B (Proc. Suppl.)* **52B** (1997) 17
11. J. Knapp et al., accepted by *Astropart. Phys.* (2002); preprint astro-ph/0206414
12. J. Ranft, *Phys. Rev.* **D51** (1995) 64; preprints hep-ph/9911213 and hep-ph/9911232 (1999) and private communications (2001)
13. M. Risse et al., *Proc. 27<sup>th</sup> Int. Cosmic Ray Conf.*, Hamburg (Germany) **2** (2001) 522